NJC

Accepted Manuscript

ROYAL SOCIETY OF CHEMISTRY

www.rsc.org/njc

Excellent Visible-Light-Driven Photocatalytic Performance of Cu_2O Sensitized $NaNbO_3$ Heterostructure

*Mingshan Fan, Bo Hu, Xu Yan, Chengjie Song, Tianjun Chen, Yi Feng, Weidong Shi**

School of Chemistry and Chemical Engineering, Jiangsu University, Zhenjiang, 212013, People's Republic of China.

* *Corresponding author. Tel.: +86 511 8879 0187*

E-mail address: swd1978@ujs.edu.cn *(W. Shi)*

Abstract

The photocatalytic activity of $Cu_2O/NaNbO_3$ (CNO) heterostructure was firstly reported in this work. Pure $NaNbO_3$ photocatalyst was synthesized via a facile hydrothermal reaction using Nb_2O_5 and NaOH as a precursors. Series of Cu_2O nanoparticles modified $NaNbO_3$ were prepared via chemical reduction of Cu salt. The composition and morphology of prepared CNO samples were characterized by variety of analytical methods. The results showed that Cu_2O nanoparticles were well distributed on the surface of cube $NaNbO_3$ micro-structure. The photocatalytic performance of prepared samples was evaluated by degradation of methyl orange (MO) under the visible light irradiation. The effect of MO degradation revealed that Cu_2O nanoparticles could act as sensitizers for improving visible light absorption of $NaNbO_3$ cube. We proposed the heterostructure between Cu_2O and $NaNbO_3$, by which the recombination of electrons and holes was efficiently inhibited as well as an enhanced photocatalytic activity.

Keywords: $NaNbO_3$, Cu_2O, Heterostructure, Photocatalyst.

1. Introduction

In recent years, the environment crisis has become the primary problem of the human development. Degradation of pollutants via semiconductor-based photocatalysts has attracted great attention for their excellent properties in solving environmental problems [1-2]. Many semiconducting photocatalysts have been developed since 1972 [3-10]. Among the various photocatalysts, n-type semiconductor sodium niobate ($NaNbO_3$) has received immense attention in the photocatalytic field for its outstanding properties, such as chemical stability, corrosion resistance and nontoxicity [11-15]. The $NaNbO_3$ with the perovskite-structure is composed by [NbO_6] octahedron that can separate the photoexcited electron-hole pairs effectively. This progress will prompt the photocatalytic activity of $NaNbO_3$ [16-19]. However, the wide bandgap of $NaNbO_3$ (Eg=3.36 eV) restricts its photo-response in the UV region due to only about 4% to 5% of solar spectrum falling in the UV range. Therefore, the effective use of visible light remains a great challenge.

By far, diverse strategies have been developed to improve the visible light absorption of $NaNbO_3$ photocatalysts, such as doping with metal and non-metal, sensitizing the photocatalyst by narrow bandgap semiconductors et al. [20-24]. Among them, sensitizing by narrow bandgap semiconductors can not only broaden the absorption region into the visible light efficiently, but also further reduce the recombine rate of electron-hole pairs [25-26]. Based on this strategy, some visible-light-driven $NaNbO_3$-based composite photocatalysts have been investigated.

For example, Lv et al. have been synthesized the In_2O_3/$NaNbO_3$ composite photocatalysts and exhibited their high-efficiency photocatalytic H_2 evolution under visible light [27]. Shi et al. have been developed g-C_3N_4/$NaNbO_3$ composite photocatalysts with enhanced visible light photocatalytic activities for the CO_2 photo-reduction [16]. Kumar et al. fabricated CdS/$NaNbO_3$ core/shell heterostructures with the high activities for photodegradation of methylene blue (MB) under visible light irradiation [6]. These reported $NaNbO_3$-based composite photocatalysts can be called the staggered bandgap type (or no p-n type junction) heterostructures.

There is another kind of hetero-photocatalysts which have been designed based on the p-n type junction theory. They were formed between the two compounds and promote the separation of electron hole pair. The p-type and n-type semiconductor can form an internal electric field which will promote the photogenerated electrons transfer from the p-type to the n-type semiconductor. Thus, the composite will greatly enhance the photocatalytic activity under the synergies of energy band and p-n type heterostructure. Cuprous oxide (Cu_2O) with a narrow band gap of 2.0 eV has been widely used to build p-n type heterostructure for improve the utilization ratio of visible light due to its excellent properties [28-32]. Wang et al. has prepared a p-Cu_2O/n-TiO_2 heterostructure photocatalyst which exhibited large photocurrent and photoconversion efficiency under both UV and visible light irradiation [30]. Hou et al has fabricated a p-Cu_2O/n-TaON heterostructure photocatalyst which showed significantly reinforce for photoelectrochemical water oxidation performance [33]. Fortunately, the appropriate valence and conduction band position of $NaNbO_3$ and

Cu_2O could accelerate the photogenerated electrons transfer by Cu_2O to the $NaNbO_3$. In addition, the composite of p-type Cu_2O and n-type $NaNbO_3$ will form a p-n type heterostructure which will be further enhance the separation rate of the electron-hole pairs. To best of our knowledge, constructing Cu_2O-$NaNbO_3$ p-n type heterostructure has not been reported

In this paper, we successfully prepared a series of CNO p-n heterostructure compound via two simple methods. In those CNO composite photocatalysts, cuprous oxide nanoparticle served as the sensitizers and facilitate the electron transfer to $NaNbO_3$, thereby separating photogenerated charge carrier s efficiently. As a result, the CNO compound has a great increase in visible light absorption and the separation rate of photogenerated electron–hole pairs. And we find a best ratio of sodium niobate and cuprous oxide by degradation of methyl orange (MO) under the visible light irradiation.

2. Experimental

All chemical reagents in this work were of analytical grade and were used without further purification.

2.1 Synthesis $NaNbO_3$

The pure $NaNbO_3$ photocatalysts were prepared by one step hydrothermal method in the following procedure：2 mmol Nb_2O_5 powder was put into 10 mL KOH (8 mol/L) and stirred for 10 min. The obtained mixture was transferred into a 15 mL of Teflon-lined stainless steel autoclave and heated at 200 °C for 12 h. After reaction, the autoclave was cooled to room temperature naturally. The resulted products were washed several times with distilled water and absolute ethanol. Finally, the power was dried at 70 °C for 12h.

2.2 Synthesis $Cu_2O/NaNbO_3$ composites

For the compounds of CNO, the $NaNbO_3$ power and the corresponding molar percentage $Cu(NO_3)_2$ (0, 4%, 6%, 8%, 10%, 15%) was dispersed in water and the reaction mixture was allowed to stir for 20 minutes. The excess $NaBH_4$ aqueous solution was added into the vigorously stirred solution for 2h under water bath. The resulting colored product was extracted by centrifugation and washed repeatedly with water and alcohol. Finally, the product was dried under vacuum at 60 ℃ for 2 h.

2.3 Characterization

The obtained products were analyzed by X-ray diffraction (XRD) patterns carried out on X-ray diffraction (Bruker D8 Advance diffractometer, 50 kV, 300 mA) with Cu-Kα radiation in the range of 5–80° at a scanning rate of 7° min^{-1}. The morphologies and size of the samples were characterized by the scanning electron microscopy (SEM) and the transmission electron microscopy (TEM). SEM images were conducted by an S-4800 field emission SEM (FESEM, Hitachi, Japan). TEM images were visualized on a F20 S-TWIN electron microscope (200 kV). An x-ray dispersive spectroscopy (EDS) was used to investigate the composition and structure of samples. X-ray photoelectron spectroscopy (XPS) measurements were analyzed using a PHI Quantum 2000 XPS system (Al Kα). The UV−vis spectra of the products were obtained from a UV–vis spectrophotometer (UV2450, Shimadzu, Japan) and the $BaSO_4$ was used as a reflectance standard.

2.4 Photocatalysis evaluation

MO was used as a model organic pollutant to evaluate the photocatalytic activity of samples under visible light irradiation. The photodegradation of MO was carried out at 308 K in a photochemical reactor which contained 50mg sample and 100 mL of 10 mg/L MO solution. To exclude the influence of physical adsorption, the reactor was kept in the dark for 30 min to reach the adsorption equilibrium. Then, a 250 W xenon lamp as the light source was located about 8 cm to one side of the containing solution, which has a glass filter to remove the UV light. The photocatalytic degradation ratio of the samples was calculated by the following formula:

$$DR=(1-\frac{A_i}{A_0})\times 100\% \quad (1)$$

In this equation, DR is on half of the photocatalytic degradation ratio, A_0 is the initial absorbency of MO after reached absorption equilibrium, while A_i is the absorbency after the photocatalytic reaction. At each time interval, photocatalysts were separated by centrifugation at 10000 rpm for 5 min, and the light absorption of clear solution for the different samples was measured by an UV-vis spectrophotometer.

3. Results and discussion

3.1 XRD analysis:

The crystal structure of the samples was investigated by XRD patterns. Fig. 1a and g showed the pure diffraction peaks of Cu_2O (JCPDS # 74-1230) and $NaNbO_3$ (CPDS # 74-2436). The main diffraction peaks at 2θ=29.6, 36.6, 42.5, 61.6 and 73.8° corresponding to the (110), (111), (200), (220), and (311) planes of $NaNbO_3$, respectively. According to the XRD patterns of CNO samples (Fig. 1b-f), the main diffraction peaks near or at 2θ=22.7, 32.5, 46.4, 52.7, 58.1 and 68.1° corresponding to the (001), (110), (002), (021), (112) and (022) planes of $NaNbO_3$, respectively. No Cu_2O peaks were detected in the XRD patterns of CNO samples which may be due to the nanoparticles in those samples are well dispersed in the surface of $NaNbO_3$ [36-38]. And compared to the pure $NaNbO_3$, there are no obvious differences in intensities and widths of the XRD peaks from the CNO samples. This result indicates that the $NaNbO_3$ crystal structure has no significant change with Cu_2O modification.

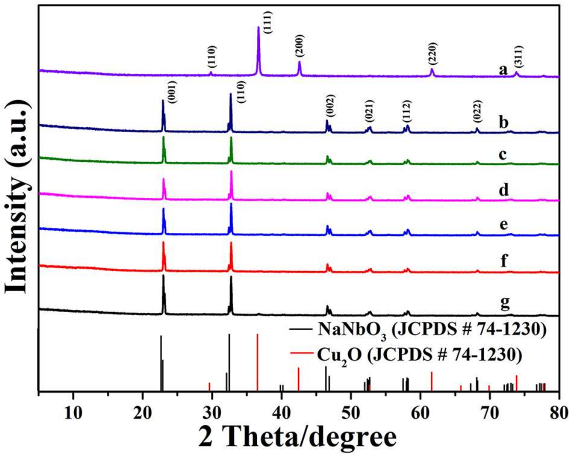

Fig. 1. X-ray diffraction patterns of (a) Cu_2O and X % CNO photocatalysts with various X: (b) X = 0; (c) X =4; (d) X = 6; (e) X =8; (f) X =10; (g) X = 15

3.2 Morphological and elements studies

The particle size and morphology of the pure $NaNbO_3$ and 8% CNO photocatalyst were measured by the SEM. Fig. 2a and b shows the SEM images of the pure $NaNbO_3$ photocatalyst which was a cube structure with the size of about 2 μm. As can be seen in those images, the $NaNbO_3$ cube possess smooth surface and no nanoparticles on it. The SEM images of the obtained 8% CNO sample shows in Fig. 2c and d. It can indicate that the Cu_2O nanoparticles were formed on the surface of the

$NaNbO_3$ cube evenly after the chemical bath deposition process. In addition, the image reveal that the CNO sample has not change the $NaNbO_3$ cube structure and the result was in accordance with their XRD patterns.

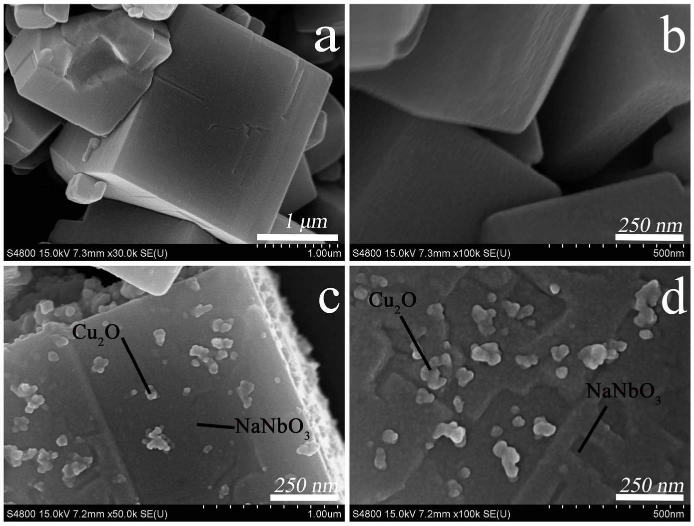

Fig. 2. SEM image of $NaNbO_3$ (a and b); SEM image of 8% CNO photocatalysts sample (c and d).

The diameter of Cu_2O nanoparticles was about 30-100 nm, as shown in TEM image (Fig. 3a and b). It is obvious that the sample was tightly integrated on the interface of Cu_2O nanoparticles and $NaNbO_3$ cube. The TEM image was well anastomotic with SEM images. To provide more solid evidence for the confirmation of heterostructure, the HRTEM image of the sample is taken and shown in Figure 3c. The *d* values of lattice spacing are measured to be 0.213 nm, matching with the spacing of the (200) crystal planes. The inset of SAED image (Fig. 3c) showed that the catalyst was multi-crystalline. Fig. 3d depicted the EDX image of the as-prepared CNO photocatalyst. Cu, Na, Nb, and O can be directly observed. In addition, the real contents of Cu atomicity (%) were calculated by EDX, which was shown in Table 1.

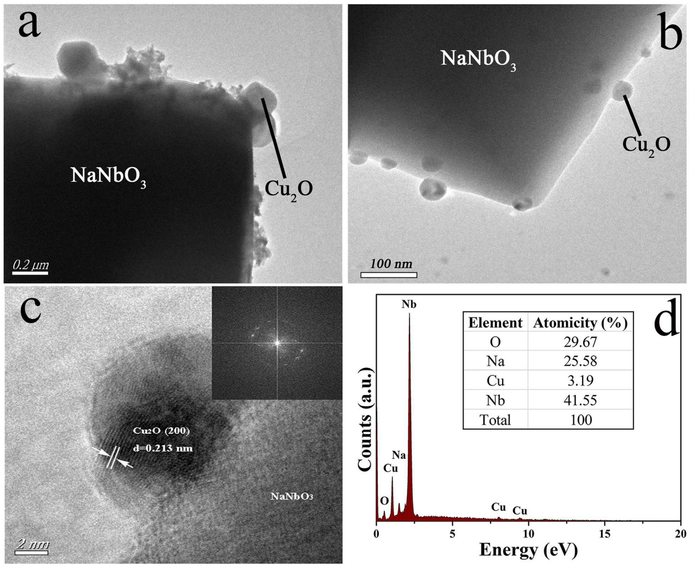

Fig. 3. TEM image of 8% CNO photocatalysts sample (a, b and c); HRTEM of 8% CNO photocatalysts sample (d). Inset: SAED image of 8% CNO photocatalysts sample.

Table 1. The real contents of all the samples.

Element atomicity (%)	NaNbO$_3$	4% CNO	6% CNO	8% CNO	10% CNO	15% CNO
Cu	0	1.26	1.76	3.19	3.31	5.01
Na	21.81	23.34	24.84	25.58	24.58	24.86
Nb	27.80	41.37	40.43	41.55	35.60	42.41
O	50.39	34.03	32.97	29.67	36.51	27.72
Total	**100**	**100**	**100**	**100**	**100**	**100**

3.3 Optical absorption studies

Fig. 4 shows the UV–vis diffuse reflectance spectra of the prepared Cu$_2$O, NaNbO$_3$ and CNO samples. The band gap energies of the pure NaNbO$_3$, Cu$_2$O samples were estimated to 3.36 eV and 2.0 eV based on the Kubelka-Munk function plot (Fig. 4b and c) [39-41]. The spectrum of CNO compounds revealed two absorption edges, which explained that the compounds contain two kinds of semiconductors ($NaNbO_3$ and Cu_2O). Moreover, integrating Cu_2O onto $NaNbO_3$ cube structure resulted in considerable red shift in the absorption onset of $NaNbO_3$ and an enhanced absorption in the visible-light region which is suggesting the interfacial interaction between the $NaNbO_3$ cube structure and Cu_2O nanoparticles [42-43]. After the $NaNbO_3$ micro-cube being covered with Cu_2O nanoparticles, a better visible light absorbance was observed on CNO compounds photocatalysts samples. Therefore, the CNO compounds photocatalysts are expected to possess better visible-light driven photocatalytic abilities.

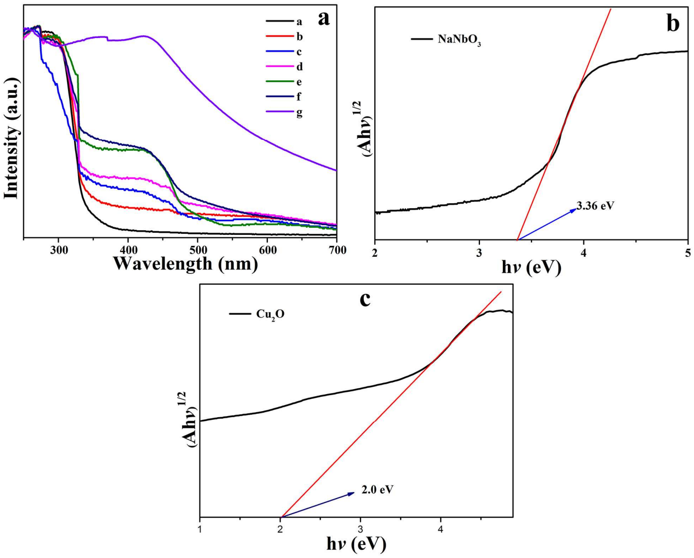

Fig. 4. a: UV–vis diffuse reflectance spectra of X % CNO photocatalysts with various X: (a) X = 0; (b) X = 4; (c) X = 6; (d) X = 8; (e) X =10; (f) X =15; (g) Cu_2O; b and c : the Kubelka-Munk function plot of $NaNbO_3$ and Cu_2O.

3.4 XPS analysis:

The surface chemical composition and the chemical state of the CNO photocatalyst sample were analyzed by the X-ray photoelectron spectroscopy (XPS) spectra. The wide scan XPS spectrum of the 8% CNO samples was shown in fig. 5a. From the XPS spectra, Cu, O, C and Nb elements were detected which farther verifies Cu element has loading on the surface of $NaNbO_3$. The emergence of the C element was mainly due to the adventitious carbon from the XPS instrument itself. Fig. 5b shows the high resolution XPS scans over Cu $2p_{3/2}$ peak. The main peak at 932.4 eV and 952.1 eV was known as the characteristic peak of Cu^+, while the shake-up satellite peaks on the higher binding energy side [44-46]. The shake-up satellite peaks indicated the presence of an unfilled Cu 3d orbit and thus demonstrated the existence of Cu^{2+} on the sample. This phenomenon was probably due to a small portion of Cu_2O that might be oxidized to CuO during the sample under normal ambient condition [47]. This state had been reported by many researchers on the synthesis of Cu_2O nanoparticles, and it had been found that a small amount of CuO on Cu_2O nanoparticle surface could actually enhance its stability. The high-resolution Nb_{3d} spectrum (206.17 eV, Fig. 5c) can be attributed to the binding energy of Nb^{5+} of the sample. The high-resolution O_{1s} peak at 528.1 eV could be attributed to the lattice oxygen species, while the signal at the 531.0 eV could be ascribed to the Cu-O in Cu_2O.

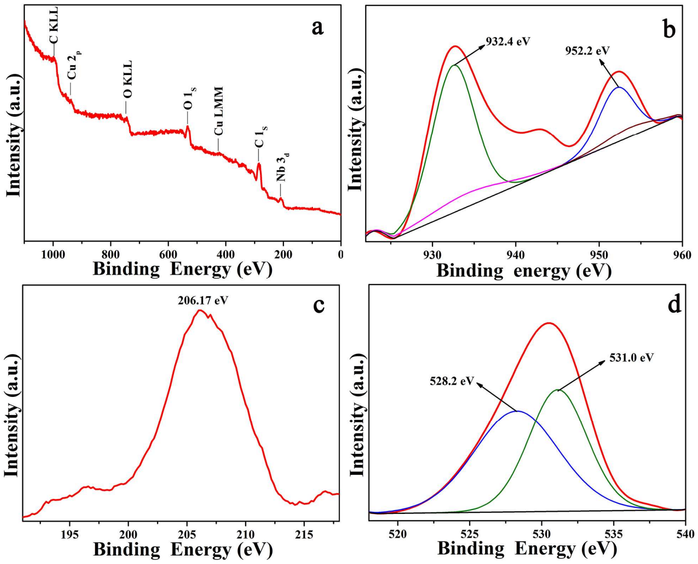

Fig. 5. XPS survey spectrum of CNO photocatalyst (a); High resolution Cu_{2p} spectrum (b); High resolution Nb_{3d} spectrum (c); High resolution O_{1s} spectrum (d);

3.5 Photocatalytic activity

The photocatalytic activities of the $NaNbO_3$ and CNO samples were evaluated by their effect of degradation MO under visible light irradiation. When there was no photocatalyst presence, a negligible amount of MO solution will be degraded under visible light irradiation attribute to its high stability. The pure $NaNbO_3$ and Cu_2O displayed weak MO removal capability under visible light irradiation due to its wide bandgap and instability, respectively, as shown in Fig. 6a and h. The degradation ratio of MO over 4% CNO photocatalyst samples was 21.23% (Fig. 6b). With the Cu_2O contents increasing, the photocatalytic activity was improved. The highest degradation rate was obtained when the contents of Cu_2O increase to 8% (Fig. 6d). For this sample, photodegradation activity was enhanced 9 times than the photocatalysts samples of Cu_2O and $NaNbO_3$ mechanical mixture with the Cu_2O content of 8% (Fig. 6g). However, the photocatalytic activity was decreased with the further loading contents of Cu_2O for CNO photocatalysts sample (Fig. 6e and f). It was possible for the photoexcited electrons in Cu_2O nanoparticles to transfer into $NaNbO_3$, more $Cu(NO_3)_2$ addition will lead to the formation of much larger Cu_2O nanoparticle covering on the surface of $NaNbO_3$ cube and then reduce the numbers of $NaNbO_3$ active sites available for photocatalytic reaction [48].

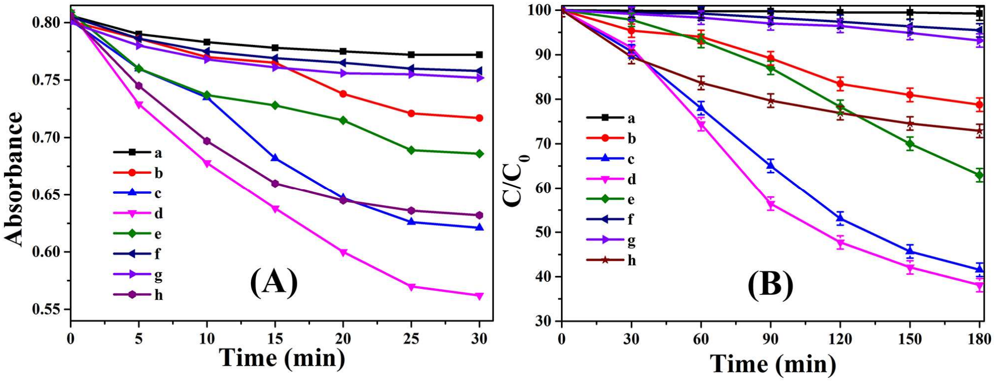

Fig. 6. Adsorption equilibrium (A) and Photocatalytic degradation (B) of MO using X % CNO photocatalysts with various X: (a) X = 0; (b) X = 4; (c) X = 6; (d) X = 8; (e) X =10; (f) X =15; (g) Cu_2O and $NaNbO_3$ mechanical mixture with the Cu content of 8 %; (h) Cu_2O.

Fig. 7 illustrated photocatalytic degradation pseudo-first-order kinetics of MO by CNO photocatalysts sample. There was a linear relationship between irradiation time and $-\ln(C/C_0)$, which indicated that the photocatalytic degradation process complies with the first-order reaction kinetic process. However, Cu_2O pseudo-first-order kinetics has poor linear correlations due to its instability. The result revealed that the degradation rate of the 8% CNO photocatalysts sample possess the highest photocatalytic activity than others.

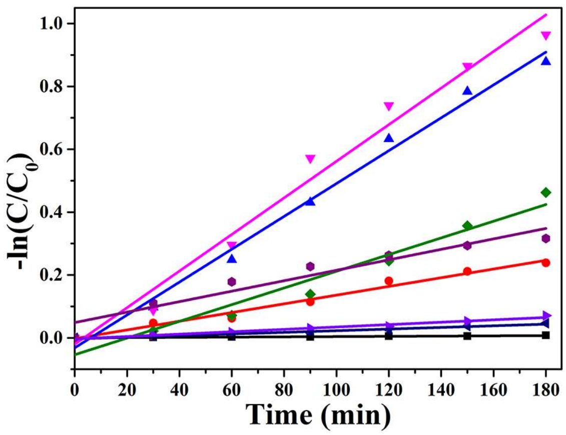

Fig. 7. The photocatalytic degradation of MO using X % CNO photocatalysts under visible light irradiation: (a) X = 0; (b) X = 4; (c) X = 6; (d) X = 8; (e) X =10; (f) X=15; (g) Cu_2O and $NaNbO_3$ mechanical mixture with the Cu content of 8 %; (h) Cu_2O.

3.6 Photocatalytic degradation mechanism

To explore the mechanism of photocatalysis using CNO composite photocatalyst, a series of experiments were made to find the ruling active species. In these experiments, t-BuOH was added to the reaction system as an hydroxyl radicals (•OH) scavenger [49-50], $K_2Cr_2O_7$ was adopted to quench of e^- [51], benzoquinone as a scavenger for superoxide radicals ($•O_2^-$) and triethanolamine as a scavenger for h^+ [52-54]. The results of trapping experiment were shown in Fig. 8.

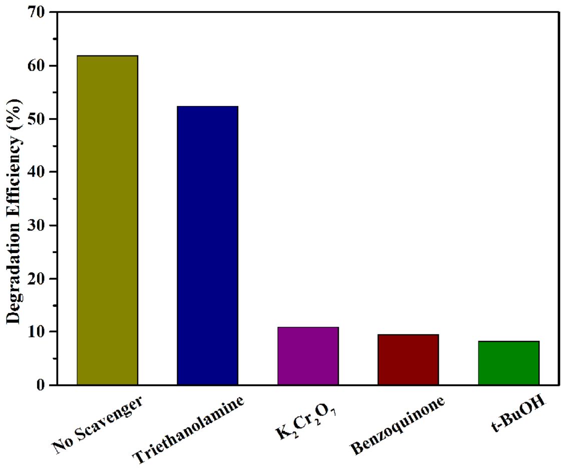

Fig. 8. Effects of a series of scavengers on the photodegradation efficiency of MO using 8 % CNO photocatalyst

The t-BuOH and $K_2Cr_2O_7$ exhibits a reduced the photodegradation of CNO photocatalysts for MO. However, the triethanolamine only has few effects on the photocatalytic reaction. Directed by the above active species trapping experimental results, the radical production could be deduced as follows: [53, 55]

$$Cu_2O + h\nu \rightarrow Cu_2O\ (e^-_{CB}) + Cu_2O\ (h^+_{VB}) \quad (2)$$

$$Cu_2O\ (e^-_{CB}) + NaNbO_3 \rightarrow Cu_2O + NaNbO_3\ (e^-_{CB}) \quad (3)$$

$$NaNbO_3\ (e^-_{CB}) + O_2 \rightarrow NaNbO_3 + \bullet O_2^- \quad (4)$$

$$\bullet O_2^- + HO_2 \rightarrow \bullet HO_2 + OH- \quad (5)$$

$$\bullet HO_2 + H_2O \rightarrow \bullet OH + H_2O_2 \quad (6)$$

$$H_2O_2 \rightarrow 2\bullet OH \quad (7)$$

$$OH\bullet + MB \rightarrow CO_2 + H_2O \quad (8)$$

Fig. 9 shows the energy band structure of the $Cu_2O/NaNbO_3$ p-n heterostructure [53, 55]. Under the irradiation of visible light, only Cu_2O was excited to produce electron-hole pairs in the CNO photocatalysts [30]. Then, the photogenerated electrons by Cu_2O can transfer to the CB of $NaNbO_3$ driven by the different band potential and the internal electric field, resulting in the aggregation of electrons in the CB of $NaNbO_3$ and photoexcited holes in the VB of Cu_2O. The aggregation of electronic in the CB of $NaNbO_3$ can be easily trapped by molecular oxygen in the reaction system to produce $\bullet O_2^-$. Thus, the separation rate of photogenerated electron–hole pairs was substantially increased. The formed $\bullet O_2^-$ will generate abundant active •OH radicals with water. And then, the MO was degraded by the •OH.

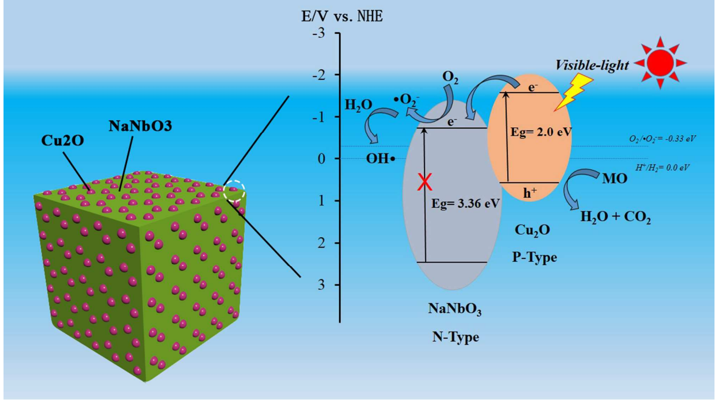

Fig. 9. Schematic illustration of the charge transfer in CNO composites.

3.7 Photoluminescence spectra (PL) studies

In order to determine the transfer and separation efficiency of the photogenerated charge carriers, the samples was characterized by Photoluminescence spectra (PL), shown in Fig. 9a. The result showed that $NaNbO_3$ had a strong emission peaks in the range of 350-380 nm and the CNO samples has weaker PL intensity than the pure $NaNbO_3$ which demonstrate that the CNO samples can suppress the electron–hole pairs recombination efficiently. In addition, the PL intensity agreed strongly with the photocatalytic reaction results [56-57]. To further prove the CNO samples had inhibited the recombination of electron-hole pairs, the transient photocurrent response was performed under visible light irradiation. As shown in Fig. 9b, a small photocurrent density was observed for pure $NaNbO_3$ when the light source was switched on. However, with loading Cu_2O on the surface of $NaNbO_3$, the transient photocurrent response was enhanced drastically. Thus, the results could demonstrate that the charge has transferred and separated effectively again.

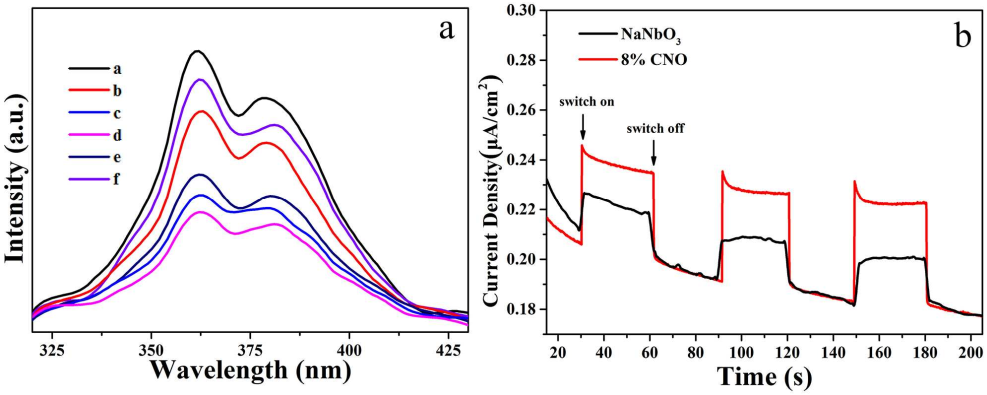

Fig.10 (a): Photoluminescence emission spectra of X % CNO photocatalysts with various X: (a) X = 0; (b) X = 4; (c) X = 6; (d) X = 8; (e) X =10; (f) X =15. (b): Photocurrent versus time (I–t) curves of the pure $NaNbO_3$ and 8 % CNO samples.

4. Conclusions

Composite $Cu_2O/NaNbO_3$ photocatalyst was synthesized by a facile reaction. A p–n heterostructure was formed by Cu_2O nanoparticle and $NaNbO_3$ cube. As a result, the best $Cu_2O/NaNbO_3$ photocatalyst can be successfully degradation the methyl orange and the photodegradation activity was enhanced 9 times than the photocatalysts samples of Cu_2O and $NaNbO_3$ mechanical mixture with the Cu_2O content of 8 %.under the irradiation of visible light. The findings indicated that Cu_2O nanoparticles could act as sensitizers for improved visible light absorption and the formed p-n heterostructure to reduce the recombination rate of electron-hole pair. This new photocatalyst promising has broad prospects in the field of environmental applications.

Acknowledgments

We gratefully acknowledge the financial support of the National Natural Science

Foundation of China (21276116, 21477050, 21301076 and 21303074), Excellent Youth Foundation of Jiangsu Scientific Committee (BK20140011), Chinese-German Cooperation Research Project (GZ1091). Program for High-Level Innovative and Entrepreneurial Talents in Jiangsu Province, Program for New Century Excellent Talents in University (NCET-13-0835), Henry Fok Education Foundation (141068) and Six Talents Peak Project in Jiangsu Province (XCL-025).

References

1. F. Zaera, *Chem. Soc. Rev.*, 2013,**42**, 2746-2762
2. M. Yang, N. Zhang, M. Pagliaro and Y. Xu, *Chem. Soc. Rev*. 2014, **43**, 8240-8254.
3. D. J. Weinberg, S. M. Dyar and Z. Khademi, *J. Am. Chem. Soc.*, 2014, **136**, 14513-14518.
4. Y. Yu, S. Huang, Y. Li, S. N. Steinmann, W. Yang and L. Cao, *Nano Lett.*, 2014, **14**, 553-558
5. J. Su, L. Guo, N. Bao and C. A. Grimes, *Nano Lett.*, 2011, **11**, 1928-1933
6. S. Kumar, S. Khanchandani, M. Thirumal and A. K. Ganguli, *ACS Appl. Mater. Inter.*, 2014, **6**, 13221-13233.
7. K. Q and S. Yang, *ACS Appl. Mater. Inter.*, 2013, **5**, 3683-3690.
8. J. Yu, J. Low and W. Xiao, *J. Am. Chem. Soc.*, 2014, **136**, 8839-8842
9. N. Zhang, Y. Zhang and Y. Xu, *Nanoscale*, 2012, **4**, 5792-5813
10. W. Zhou, W. Li and J. Wang, *J. Am. Chem. Soc.*, 2014, **136**, 9280-9283
11. K. Saito and A. Kudo, *Inorg. Chem.*, 2010, **49**, 2017-2019.
12. H. Shi, X. Li, D. Wang, Y. Yuan, Z. Zou and J. H. Ye, *Catal. Lett.* 2009, **132**, 205-212.
13. P. Li, H. Xu, L. Liu, T. Kako, N. Umezawa, H. Abe and J. Ye, *J. Mater. Chem. A.*, 2014, **2**, 5606-5609.
14. N. Chen, G. Li and W. Zhang, *Physica B.*, 2014, **447**, 12-14.
15. X. Li, G. Li, S. Wu, X. Chen and W. Zhang, *J. Phys. Chem. Solids.*, 2014, **75**, 491-494.
16. H. Shi, G. Chen, C. Zhang and Z, Zou, *ACS Catal.*, 2014, **4**, 3637-3643
17. G. Li, Z. Yi, Y. Bai, W. Zhang and H. Zhang, *Dalton Trans.*, 2012, **41**, 10194-10198
18. P. Li, S. Ouyang, G. Xi, *J. Phys. Chem. C.*, 2012, **116**, 7621-7628.
19. K. Katsumata, C. E. J. Cordonier, T. Shichi and A. Fujishima, J. Am. C*hem. Soc.*, 2009, **131**, 3856-3857
20. J. Lv, T. Kako, Z. Li, Z. Zou and J. Ye, *J. Phys. Chem. C.*, 2010, **114**, 6157-6162.
21. S. A. Ansari, M. M. Khan, M. O. Ansari, J. Lee and M. H. Cho, *New J. Chem.*, 2014, **38**, 2462–2469.
22. Y. Wang, R. Shi, J. Lin and Y. Zhu, *Energy Environ. Sci.*, 2011, **4**, 2922-2929.

23. C. Han, M. Yang, B. Weng and Y. Xu, *Phys. Chem. Chem. Phys.*, 2014, **16**, 16891—16903
24. F. Dong, Q. Li, Y. Zhou, Y. Sun, H. Zhang and Z. Wu, *Dalton Trans.*, 2014, **43**, 9468-9480
25. S. Bai, L. Wang, X. Chen, J. Du and Y. Xiong, *Nano Research*, 2015, **8**, 175-183.
26. W. Zhang, Y. Sun, F. Dong, W. Zhang, S. Duan and Q. Zhang, *Dalton Trans.*, **2014**, 43, 12026-12036.
27. J. Lv, T. Kako, Z. Li, Z. Zou and J. Ye, *J. Phys. Chem. C.,* 2010, **114**, 6157-6162.
28. D. J. Weinberg, S. M. Dyar and Z. Khademi, *J. Am. Chem. Soc.*, 2014, **136**, 14513-14518.
29. Y. Bu and Z. Chen, *RSC Adv.*, 2014, **4**, 45397-45406
30. M. Wang, L. Sun, Z. Lin, J. Cai, K. Xie and C. Lin, *Energy Environ. Sci.*, 2013, **6**, 1211-1220.
31. A. Paracchino, N. Mathews, T. Hisatomi, M. Stefik, S. Tilley and M. Gratzel, *Energy Environ. Sci.*, 2012, **5**, 8673-8681
32. S. Deng, V. Tjoa, H. M. Fan, H. R. Tan, D. C. Sayle, M. Olivo, S. Mhaisalkar, J. Wei and C. H. Sow, *J. Am. Chem. Soc.*, 2012, **134**, 4905-4907.
33. J. Hou, C. Yang, H. Cheng, S. Jiao, O. Takeda and H. Zhu, *Energy Environ. Sci.*, 2014, **7**,3758-3768
34. J. Lee, K. You and C. Park. *Adv. Mater.*2012, **24**, 1084-1088.
35. W. Xu, X. Liu, J. Ren, P. Zhang, Y. Wang, Y.G. Guo and G. Lu, *Catal. Commun*, 2010, **11**, 721-726.
36. Z. Zhao, X. Lin, R. Jin, Y. Dai and G. Wang, *Catal. Commun*, 2011, 12, 1448-1451.
37. F. X, *ACS Appl. Mater. Inter.*, 2012, **4**, 7055-7063.
38. P. Madhusudan, J. R. Ran, J. Zhang, J. G. Yu and G. Liu, *Appl. Catal. B.*, 2011, **110**, 286-295.
39. H. Fan, H. Li, B. Liu, Y. Lu, T. Xie and D. Wang, *ACS Appl. Mater. Inter.,* 2012, **4**, 4853-4857
40. W. Ong, L. Tan, S. Chai, S. Yong, A. Mohamed, *Nano Energy*, 2015, doi:10. 1016/j. nanoen. 2015. 03. 014
41. T. Wang, X. Meng, P. Li, S. Ouyang, K. Chang, G. Liu, Z. Mei, J. Ye, *Nano Energy*, 2014, **9**, 50–60.
42. X. Qiu, M. Miyauchi, K. Sunada, M. Minoshima, M. Liu, Y. Lu, D. Li, Y. Shimodaira, Y. Hosogi, Y. Kuroda and K. Hashimoto, *ACS Nano.*, 2012, **6**, 1609-1618.
43. Q. Sun, Y. Li, X. Sun, L. Dong, *ACS Sustain. Chem. Eng.*, 2013, **1**, 798-804.
44. T. Ghodselahi, M. A. Vesaghi, A. Shafiekhani, A. Baghizadeh and M. Lameii, *Appl. Surf. Sci.*, 2008, **255**, 2730-2734.
45. H. Liu, J. Wang, X. Fan, F. Zhang, H. Liu, J. Dai and F. Xiang, *Mater. Sci. Eng. B.* 2013, **178**, 158-166.
46. Y. D. Hou, A. B. Laursen, J. S. Zhang, G. G. Zhang, Y. S. Zhu, X. C. Wang, S. Dahl and I. Chorkendorff, *Angew. Chem. Int. Edit.*, 2013, **52**, 3621-3625.
47. L. Q. Ye, J. Y. Liu, C. Q. Gong, L. H. Tian, T. Y. Peng and L. Zan, *ACS Catal.* 2012, **2**,

1677–1683.

48. C. H. Zhang, L. H. Ai, L. L. Li and J. Jiang, *J. Alloy. Compd.* 2014, **582**, 576-582.
49. X. Yan, X. Wang, W. Gu, M. Wu, Y. Yan, B. Hu, G. Che, D. Han, J. Yang, W. Fan, W. Shi, *Appl. Catal. B*, 2015, **164**, 297–304
50. Z. Chen, N. Zhang and Y. Xu, *CrystEngComm*, 2013, **15**, 3022–3030
51. S. Kumar, S. Khanchandani, M. Thirumal and A. K. Ganguli, *ACS Appl. Mater. Inter.*, 2014, **6**, 13221-13233.
52. Y. Wang, K. Deng and L. Zhang, J. P*hys. Chem. C*, 2011, **115**, 14300-14308.
53. L. Yang, S. Luo, Y. Li, Y. Xiao, Q. Kang, and Q. Cai, *Sci. Technol.* 2010, **44**, 7641-7646.
54. N. Zhang, M. Yang, Z. Tang and Y. Xu, *ACS Nano.*, 2014, **8**, 623-633.
55. Y. Hou, X. Y. Li, Q. D. Zhao, X. Quan and G. H. Chen, *Appl. Phys. Lett.* 2009, **95**, No. 093108.
56. W. Ong, L. Tan, S. Chai and S. Yong, *Chem. Commun.*, 2015, **51**, 858-861
57. L. Zhang, W. Wang, D. Jiang, E. Gao and S. Sun, *Nano Research*, 2015, **8**, 821-831

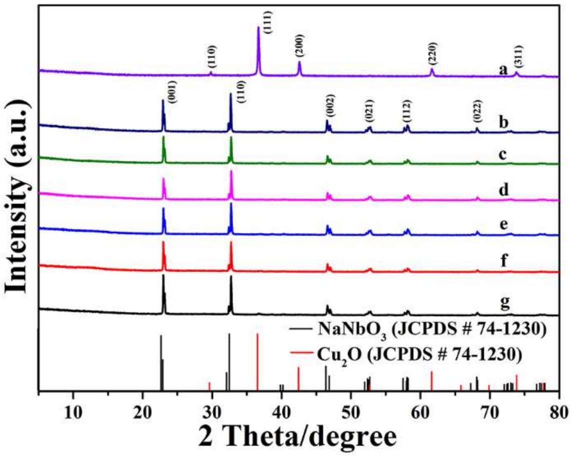

Fig. 1. X-ray diffraction patterns of (a) Cu_2O and X % CNO photocatalysts with various X: (b) X = 0; (c) X =4; (d) X = 6; (e) X =8; (f) X =10; (g) X = 15

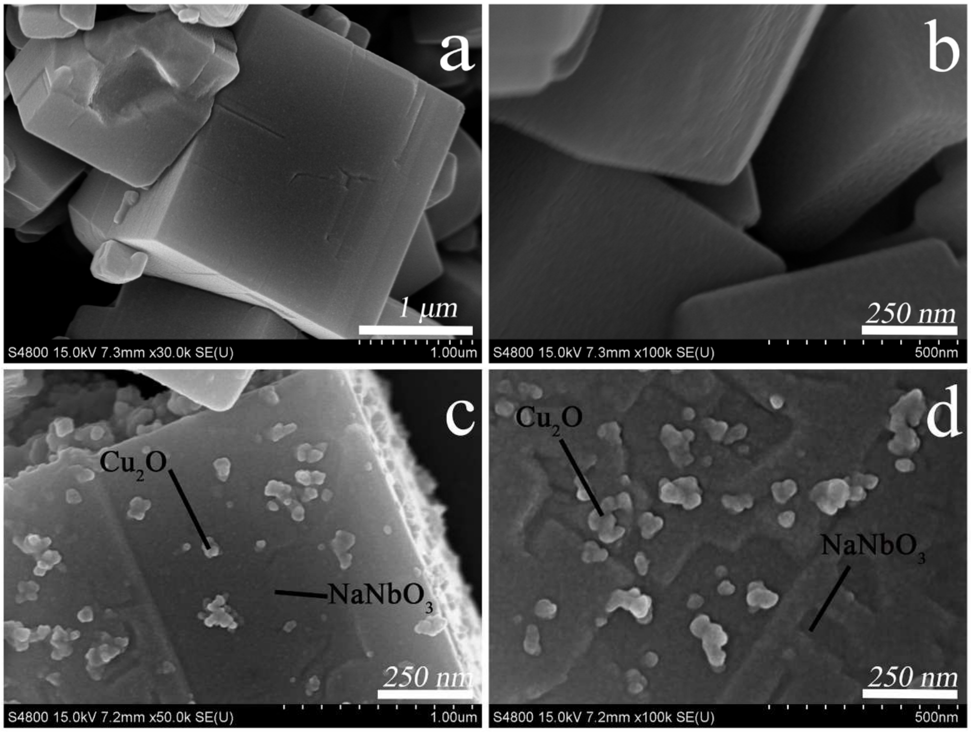

Fig. 2. SEM image of $NaNbO_3$ (a and b); SEM image of 8% CNO photocatalysts sample (c and d).

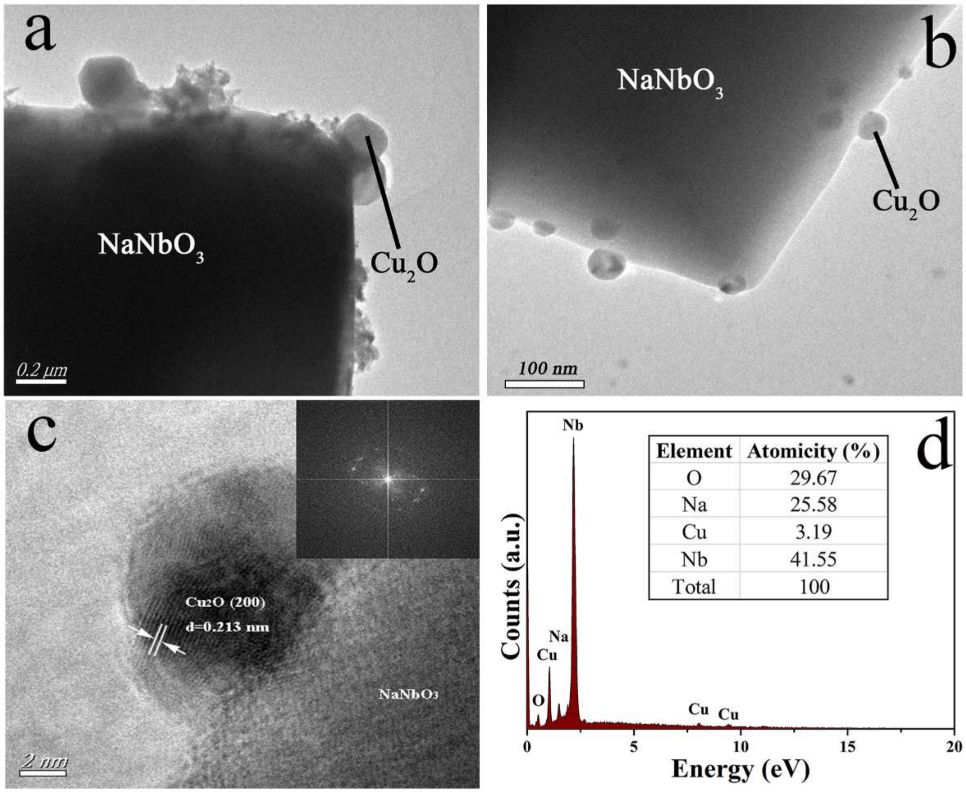

Element	Atomicity (%)
O	29.67
Na	25.58
Cu	3.19
Nb	41.55
Total	100

Fig. 3. TEM image (a and b); HRTEM (c); Inset: SAED image. EDX (d) of 8% CNO photocatalysts sample.

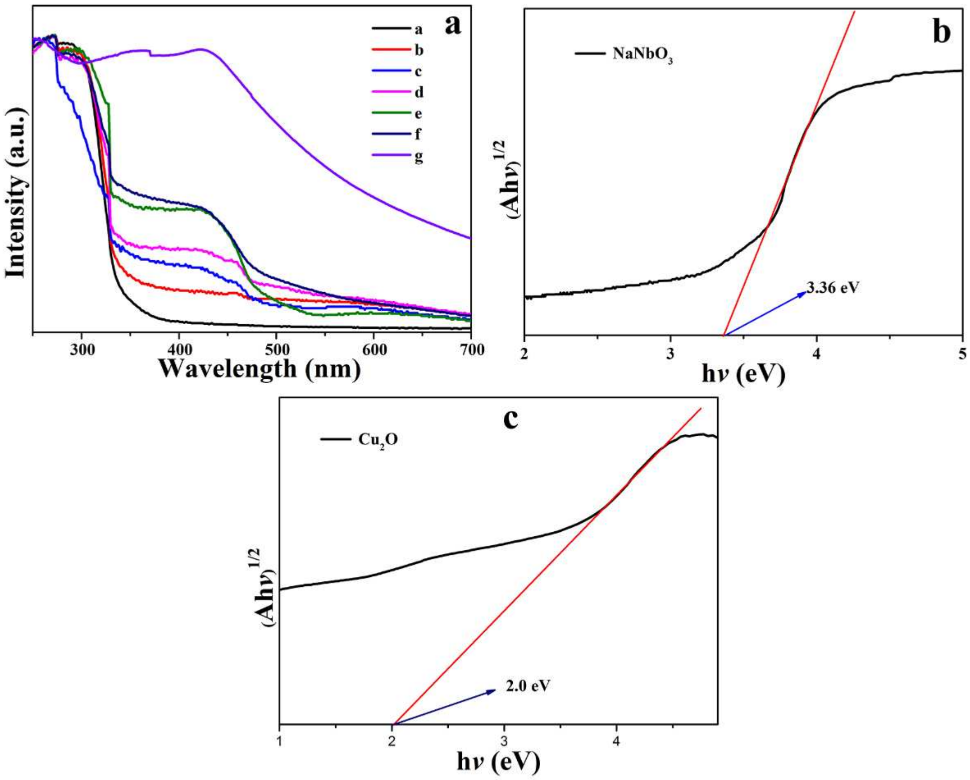

Fig. 4. a: UV–vis diffuse reflectance spectra of X % CNO photocatalysts with various X: (a) X = 0; (b) X = 4; (c) X = 6; (d) X = 8; (e) X =10; (f) X =15; (g) Cu_2O; b and c : the Kubelka-Munk function plot of $NaNbO_3$ and Cu_2O.

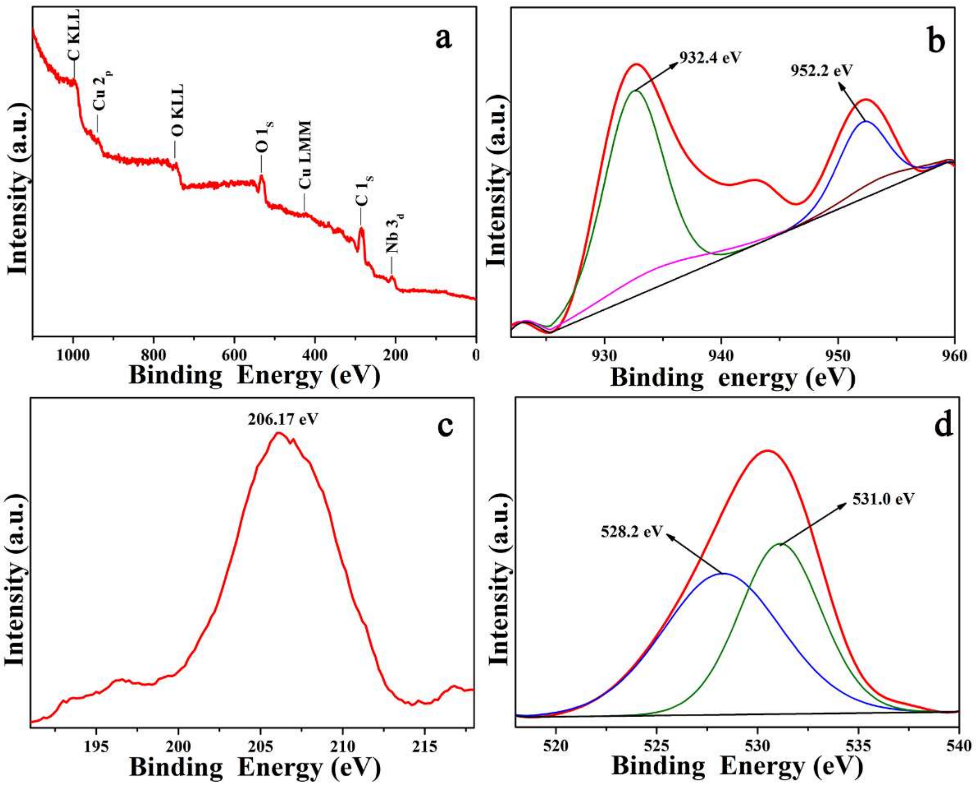

Fig. 5. XPS survey spectrum of CNO photocatalyst (a); High resolution Cu_{2p} spectrum (b); High resolution Nb_{3d} spectrum (c); High resolution O_{1s} spectrum (d).

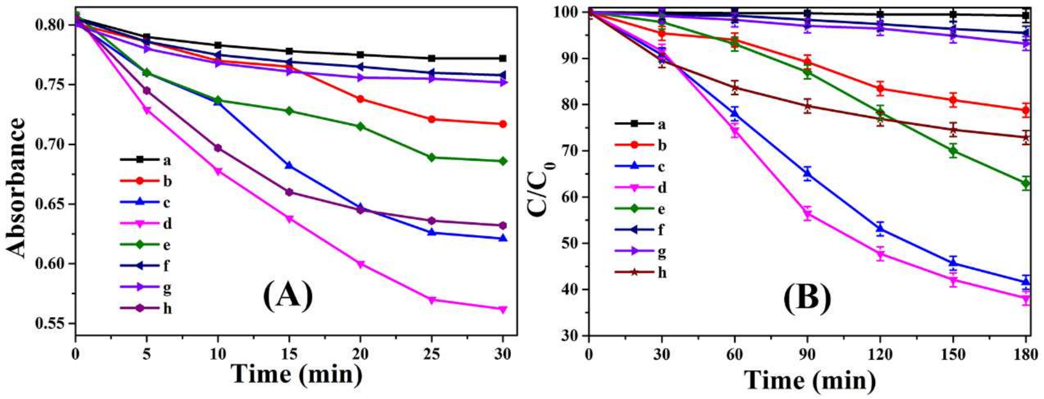

Fig. 6. Adsorption equilibrium (A) and Photocatalytic degradation (B) of MO using X % CNO photocatalysts with various X: (a) X = 0; (b) X = 4; (c) X = 6; (d) X = 8; (e) X =10; (f) X =15; (g) Cu_2O and $NaNbO_3$ mechanical mixture with the Cu content of 8 %; (h) Cu_2O.

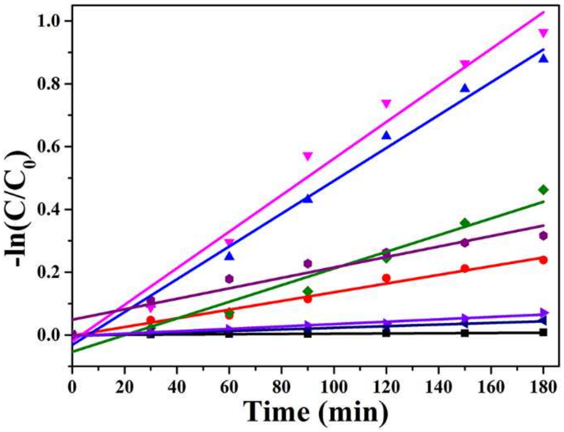

Fig. 7. The photocatalytic degradation of MO using X % CNO photocatalysts under visible light irradiation: (a) X = 0; (b) X = 4; (c) X = 6; (d) X = 8; (e) X =10; (f) X=15; (g) Cu_2O and $NaNbO_3$ mechanical mixture with the Cu content of 8 %; (h) Cu_2O.

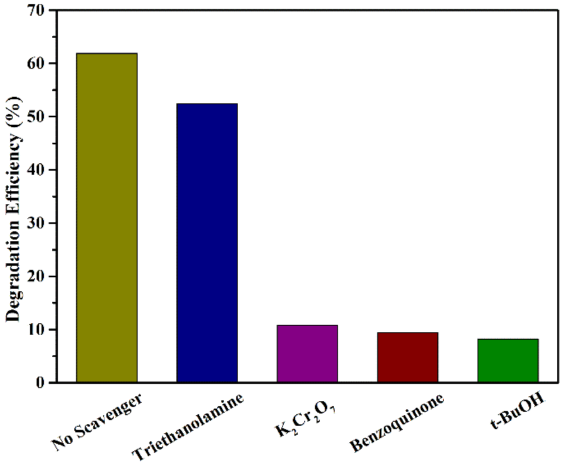

Fig. 8. Effects of a series of scavengers on the photodegradation efficiency of MO using 8 % CNO photocatalyst

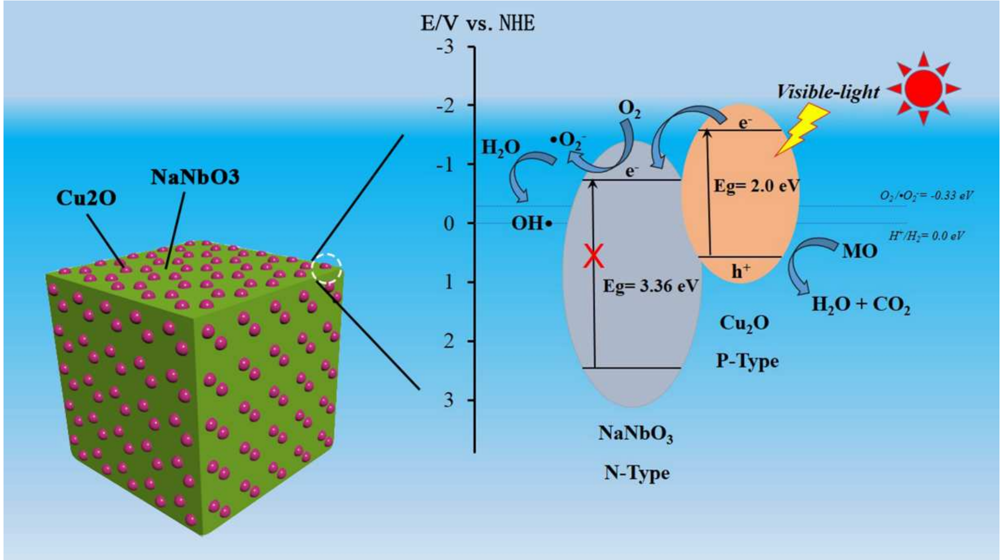

Fig. 9. Schematic illustration of the charge transfer in CNO composites.

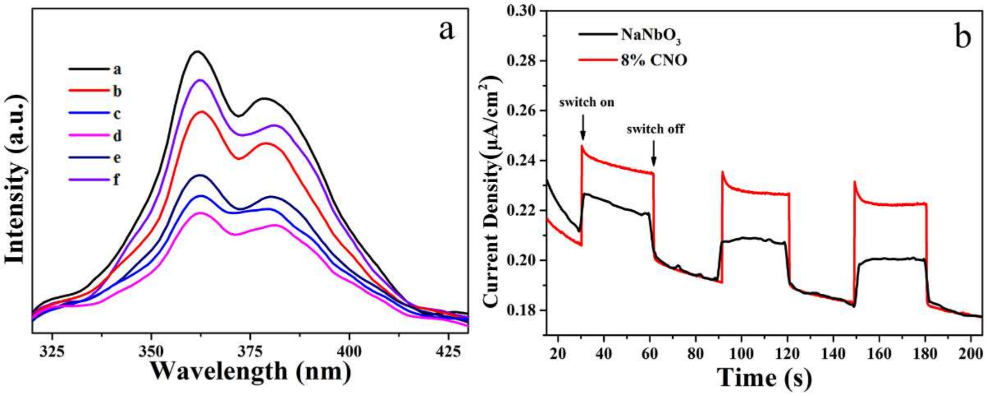

Fig.10 (a): Photoluminescence emission spectra of X % CNO photocatalysts with various X: (a) X = 0; (b) X = 4; (c) X = 6; (d) X = 8; (e) X =10; (f) X =15. (b): Photocurrent versus time (I–t) curves of the pure NaNbO$_3$ and 8 % CNO samples.

The heterostructures complexes $Cu_2O/NaNbO_3$ exhibited high catalytic activities on degradation of methyl orange.